Journal of Catalysis 273 (2010) 257–265

Contents lists available at ScienceDirect

Journal of Catalysis

journal homepage: www.elsevier.com/locate/jcat

The effect of reaction conditions on the stability of $Au/CeZrO_4$ catalysts in the low-temperature water–gas shift reaction

H. Daly [a], A. Goguet [a], C. Hardacre [a,*], F.C. Meunier [b], R. Pilasombat [a], D. Thompsett [c]

[a] CenTACat and School of Chemistry and Chemical Engineering, Queen's University Belfast, Belfast BT9 5AG, Northern Ireland, UK
[b] LCS, Univ. Caen, CNRS 6 Bd Maréchal Juin, F-14050 Caen, France
[c] Johnson Matthey Technology Centre, Blounts Court, Sonning Common, Reading RG4 9NH, UK

ARTICLE INFO

Article history:
Received 9 March 2010
Revised 24 May 2010
Accepted 30 May 2010
Available online 26 June 2010

Keywords:
Water–gas shift
Gold
Deactivation
Low temperature
Feed
DRIFTS

ABSTRACT

$Au/CeZrO_4$ catalysts are highly active for the water–gas shift reaction but tend to be unstable and deactivate with time on stream. In this study, *in situ* DRIFTS-GC was used to investigate the nature of the Au under a range of reaction conditions as the deactivation rate is observed to vary with feed conditions (water concentration, presence of CO_2) and reaction temperature. An analysis of the Au–CO bands during the reaction showed that the rate of change in the Au^0–CO bands correlated with the deactivation rate under all conditions. Although $Au^{\delta+}$–CO species may be highly active they are very unstable under the feed and, from a comparison of the behaviour of the Au–CO species under varied feeds and reaction temperatures, it is proposed that metallic gold is the predominant active state in these catalysts for low-temperature WGS reaction.

Through varying the feed conditions of the water–gas shift reaction, it was possible to enhance the stability of the catalysts significantly. Following a pre-treatment of the catalyst under the full water–gas shift feed (2% CO, 2% CO_2, 8.1% H_2 and 7.5% H_2O) and removal of CO_2 from this feed, the catalyst was found to be very stable. The extent of deactivation can be altered by varying the feed conditions during a reaction. The discovery of a way to enhance Au catalyst stability for the low-temperature water–gas shift reaction has significant implications for the development and use of these catalysts.

1. Introduction

$Au/CeZrO_4$ catalysts have been reported to be highly active for the low-temperature water–gas shift reaction which makes them interesting candidates for a range of applications including feed gas cleanup for low-temperature fuel cells [1]. However, the commercial application of these catalysts has been hindered by their tendency to deactivate rapidly under reaction conditions. The long-term stability is an important issue when catalysts are to be implemented in commercial WGS applications; therefore, an understanding of the deactivation mechanisms is critical in designing new catalysts/processes able to achieve clean hydrogen production *via* the WGS reaction. The physical origin and mechanism of the deactivation of supported Au catalysts are still controversial with the formation of formate/carbonate species [2–6], sintering of Au [7], loss of ceria supported surface area due to weakening of the gold–ceria interaction [8] and loss of the contact between the Au and the support [9] all being reported.

Previous work in our laboratory investigated the deactivation of a highly active 2 wt.% $Au/CeZrO_4$ catalyst under WGS conditions [9]. Therein, the deactivation of the catalyst was shown to be dependent on the concentration of water in the gas phase and the reaction temperature with significant thermal deactivation occurring at temperatures above 250 °C. Considering both experimental results and theoretical calculations, sintering of the Au and the build-up of carbon-containing material were not thought to be relevant and a common deactivation mechanism was proposed in which water and the reaction temperature caused dewetting of the Au nanoparticle from the support reducing the metal support interaction which is critical for the high activity of these catalysts.

In the present work, DRIFTS with on-line GC monitoring of the CO conversion has been used to probe the deactivation of $Au/CeZrO_4$ catalysts under a range of feed conditions, pre-treatments and at different reaction temperatures. DRIFT spectroscopy has been used to assess the species adsorbed on the catalyst surface under reaction conditions with particular focus on the Au carbonyl region. Infrared spectroscopy has been widely used to characterise the oxidation/coordination state of Au through analysis of the carbonyl band position and the nature of the active Au species for the WGS reaction is still much debated with both cationic Au [6,8,10] and metallic Au [11–13] proposed as the active species. Goguet et al. [9] reported a

* Corresponding author. Fax: +44 28 9097 4687.
E-mail address: c.hardacre@qub.ac.uk (C. Hardacre).

0021-9517/$ - see front matter © 2010 Elsevier Inc. All rights reserved.
doi:10.1016/j.jcat.2010.05.021

change in the CO adsorption properties of the Au nanoparticle with the Au carbonyl band intensity decreasing with time on stream. The aim of this study was to examine the correlation between the deactivation rate and the Au–CO band intensity in order to clarify the nature of the active Au species for the WGS reaction.

2. Experimental

2.1. Catalyst preparation

Using the deposition–precipitation method, 1 wt.% $Au/CeZrO_4$ catalysts was prepared . The $CeZrO_4$ (Johnson Matthey) support was slurried in water and heated to 60 °C with the pH adjusted to 8.0 by the addition of Na_2CO_3 (0.05 M). Then, 1.2 mM of $HAuCl_4$ (49.2 wt.% Au) was prepared and pumped into the stirred slurry at 10 cm^3 min^{-1}. The pH was monitored throughout using a TitraLab TIM856 pHstat (Radiometer analytical), and excess Na_2CO_3 was added to maintain the pH at 8.0. After the addition of the gold salt, stirring was continued for a further hour at 60 °C. The catalyst was recovered by filtration, thoroughly washed to remove soluble chloride and vacuum dried at room temperature for 6 h. The average particle size of the Au for catalysts prepared by this method was determined to be between 0.75 and 1 nm from STEM-HAADF images (see Supplementary Information).

2.2. Activity testing

The catalyst was tested in a plug flow tube microreactor held in a temperature-controlled furnace. The catalyst bed consisted of 50 mg of catalyst between two plugs of quartz wool and a thermocouple measured the temperature in the middle of the catalyst bed. Both reactants and products were analysed by GC (Perkin Elmer; Auto System XL ARNEL) fitted with a thermal conductivity detector. Aera mass flow controllers were used to control the flow (total flow 100 cm^3 min^{-1}) of CO, CO_2, H_2 and He to the reactor. The purity of the gases was >99.95% (supplied by BOC); dry ice/acetone traps were used on CO gas lines remove any metal carbonyl contaminants that can be found in CO cylinders. A stable flow of water vapour to the reactor was established by passing the combined flow of CO, CO_2 and H_2 through a saturator/condenser system. The saturator consisted of a 200 cm^3 heated stainless steel vessel filled with deionised water through which the permanent gases were bubbled. The temperature of the saturator was maintained at a slightly higher temperature than that required to give a water vapour pressure of 7.5 kPa. The excess water vapour from the saturator was removed in a glass condenser set at the correct temperature to deliver a constant stream containing 7.5 kPa of water vapour to the reactor. The combined saturator/condenser system gave very stable water flows required for accurate analysis of the WGS reaction. The catalyst was heated at 1 °C min^{-1} to 100 °C under He and then from 100 °C to 150 °C under the WGS feed which consisted of 2% CO, 2.5% CO_2, 8.1% H_2 and 7.5% H_2O, balance He. These feed conditions were also used when investigating the effect of reaction temperature. The reaction temperature was cycled between 150 and 400 °C over a 20-h period while monitoring the CO conversion to assess how the reaction temperature affected the activity and stability of the catalyst.

When varying the feed composition, reactions were performed in a feed without H_2 or CO_2 and also with varying amounts of water in the feed (1% H_2O or 7.5% H_2O). The total flow rate was maintained at 100 cm^3 min^{-1} by balancing the He concentration of the flow. These feed conditions are referred to as a "CO_2-free feed", a "H_2-free feed", "low water feed" (1% H_2O) and "full WGS feed" (7.5% H_2O) thereafter. The H_2 and CO_2-free feeds refer to feeds where H_2 and CO_2, respectively, have been removed from the initial gas composition. It should be noted that during the reaction H_2 and CO_2 will be formed and therefore the reactions are not completely in the absence of these components but conditions where lower amounts of H_2 and CO_2 and H_2 will be present relative to the full WGS feed used in this study which contains 8.1% H_2 and 2.5% CO_2.

The effect of pre-treating the catalyst with different components of the WGS feed was also tested. The catalyst was heated at 2 °C min^{-1} to 100 °C under He before introducing the respective pre-treatment gases. The temperature was further ramped to 200 °C under the pre-treatment gases where it was held for 1 h before switching to He and cooled to 100 °C (2 °C min^{-1}). Once at 100 °C the reaction feed was introduced and the temperature ramped at 1 °C min^{-1} to 150 °C. The pre-treatments tested include the full WGS feed, 10% H_2, 10% H_2O, 10% CO_2, 7.5% H_2O + 5% CO_2 and 7.5% H_2O + 10% CO_2. An *ex situ* pre-treatment with carbonic acid was also performed to investigate whether the deactivation could be due to the *in situ* reaction of water and carbon dioxide to form carbonic acid. The 1 wt.% $Au/CeZrO_4$ catalyst was treated with synthesised carbonic acid at room temperature. 1g of catalyst was soaked with 20 cm^3 of deionised water to form a slurry into which 40 cm^3 min^{-1} of pure CO_2 was bubbled for 30 min under continuous stirring. The resulting catalyst was filtered and dried under vacuum at room temperature for 6 h before undergoing the same reaction as detailed above following the *in situ* pre-treatments.

2.3. DRIFTS measurements

DRIFTS with on-line GC was used to monitor the surface of the catalyst (50 ± 5 mg) and the activity during the WGS reaction at 150 °C. The activity profiles obtained in the plug flow reactor and the DRIFTS-GC setup were comparable. All the activity data shown, except for in Fig. 7, result from the operando DRIFTS-GC experiments. The DRIFT spectra were recorded using a Bruker Equinox 55 spectrometer using an average of 128 scans and a resolution of 4 cm^{-1}. The DRIFTS setup consisted of an *in situ* high-temperature diffuse reflectance IR cell (Spectra-Tech) fitted with ZnSe windows which was modified in house to behave as a plug flow reactor, the details of which have been previously reported [14,15]. DRIFTS-GC experiments were performed while varying the reaction temperature and under varied feed conditions of a full WGS feed, a low water feed, a WGS feed without CO_2 and also following a pre-treatment under the full WGS feed.

The effect of the amount of water in the feed on catalyst stability was investigated. The catalyst was heated at 1 °C min^{-1} under argon to 100 °C before introduction of the WGS feed which contained either 7.5% or 1.0% water; the temperature was then further increased to 150 °C. The reaction was monitored for 20 h with spectra recorded every 30 min.

The effect of temperature on catalyst stability was also tested under the full WGS feed (7.5% H_2O). The catalyst was heated at 1 °C min^{-1} to 100 °C under argon before introduction of the WGS feed. The temperature was further increased under the WGS feed to 150 °C and held at this temperature for 1 h. The temperature was then increased to 400 °C and held at 400 °C for 1 h before returning to 150 °C. This temperature cycle was repeated over a 24-h period with infrared spectra recorded every 15 min while the temperature was held at 150 °C.

2.4. Isosteric heat of adsorption

The isosteric heat of adsorption of CO was obtained using the Clausius–Clapeyron equation from the infrared data obtained over an active and deactivated $Au/CeZrO_4$ catalyst. In these experiments,

2 wt.% Au loading was used to provide more intense Au–CO bands which aided the analysis from increased signal to noise, in particular for the deactivated catalyst. A pellet of the 2 wt.% Au/$CeZrO_4$ catalyst (30 mg) was loaded into a variable temperature transmission cell (Specac). The background spectrum of the fresh catalyst under helium at 25 °C was recorded before exposing the catalyst to the full WGS feed at 150 °C for 30 min to activate the catalyst. Following purging of the cell with helium, adsorption of *x*% CO in He (x = 0.25, 1, 4 and 8, total flow rate 200 cm^3 min^{-1}) was performed at 40 °C, 60 °C and 80 °C. The same catalyst pellet was then exposed again to the full feed at 150 °C for 12 h which resulted in deactivation of the catalyst. The 2 wt.% Au/$CeZrO_4$ catalyst lost ~30% activity following 12 h of reaction in the microreactor. The cell was purged again with helium and then cooled to 40 °C. Adsorption of the same concentrations of CO was performed on the deactivated catalyst at 0 °C, 20 °C and 40 °C. CO adsorption was performed at lower temperatures for the deactivated catalyst due to the weaker intensity of the Au–CO compared with the active catalyst.

2.5. Analysis of IR spectra

All DRIFT spectra are displayed as log 1/*R*, where *R* is the relative reflectance (*R* = reflectance recorded under WGS feed/reflectance recorded under Ar). DRIFT spectra are reported as log 1/*R* as the relative reflectance of the Au/$CeZrO_4$ catalyst under the WGS feed is greater than 60% and under these conditions log 1/*R* is proportional to surface concentration of adsorbates [16,17]. All spectra have been corrected for contributions due to unreacted gas-phase CO and the electronic transition from reduced ceria [18–20] prior to analysis with the presence of the electronic transition confirmed from ^{13}CO experiments [21]. The experiments were also carried out using a ^{13}CO feed (2% ^{13}CO, 2.5% CO_2, 8.1% H_2 and 7.5% H_2O, balance He). The shift of the Au–^{13}CO bands to lower wavenumber allowed assessment of the ceria electronic transition band at ~2125 cm^{-1} which along with the gas-phase CO bands were subtracted from all spectra using Bruker OPUS software prior to analysis.

Several overlapping features exist in the Au–CO band region and, therefore, to analyse the rate of change of the different Au species with time on stream, the spectra were deconvoluted by fitting four Gaussian curves to the data and integrating the fitted Gaussians (see Supplementary Information). The same analysis was performed on all spectra recorded under the series of reaction conditions used in this study. Normalised rate of change of Au–CO bands has been plotted to allow comparison with rate of deactivation.

3. Results and discussion

3.1. Full WGS feed conditions – activity

The stability of 2 wt.%, 1 wt.% and 0.2 wt.% Au/$CeZrO_4$ catalysts during reaction under the full WGS feed at 150 °C is shown in Fig. 1. Under the full WGS feed, all catalysts exhibit similar long-term deactivation profiles with deactivation rates of 0.23% h^{-1}. Some differences were observed for the 2 wt.% Au catalyst in that it exhibits a faster initial deactivation, over the first 100 min, before deactivating at a slower rate which is comparable with the lower loaded catalysts. Fig. 2 shows the DRIFT spectra recorded under the WGS feed at 150 °C as a function of Au loading. In each case, the same Au–CO bands were observed which shows that the loading does not alter the types of Au species formed during the reaction but only their relative proportion. The activity (rate of CO conversion) of the 2 wt.%, 1 wt.% and 0.5 wt.% Au/$CeZrO_4$ catalysts for reaction at 150 °C were found to be 520, 270 and 180 cm^3 g^{-1} h^{-1}, respectively.

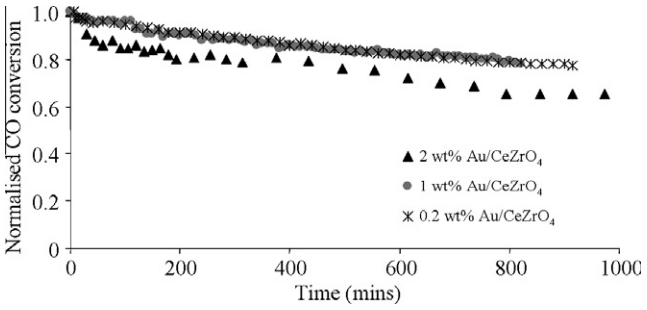

Fig. 1. Normalised CO conversion for reaction under the full WGS feed at 150 °C (2% CO, 2% CO_2, 8.1% H_2 and 7.5% H_2O) of 0.2 wt.%, 1 wt.% and 2 wt.% Au/$CeZrO_4$ catalysts.

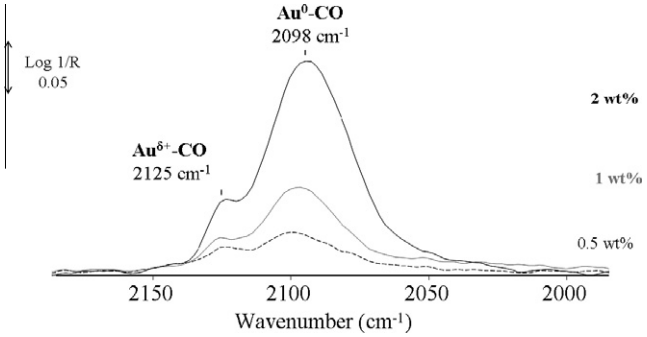

Fig. 2. DRIFT spectra (2250–1950 cm^{-1} region) recorded of 2 wt.%, 1 wt.% and 0.5 wt.% Au/$CeZrO_4$ catalysts under the full WGS feed (2% CO, 2% CO_2, 8.1% H_2 and 7.5% H_2O) at 150 °C. All spectra have been corrected for unreacted gas-phase CO and the electronic transition of reduced ceria.

3.2. Infrared analysis: DRIFT spectra under WGS feed

DRIFT spectroscopy has been used to probe the cause of Au/$CeZrO_4$ deactivation through analysis of surface species formed on the catalyst under realistic WGS reaction conditions. Fig. 3 shows DRIFT spectra of a 1 wt.% Au/$CeZrO_4$ upon introduction of the WGS feed at 150 °C and after 10 h on stream. Under this feed, bands due to bidentate formates are observed (OCO vibration: ν_{as} at 1588 cm^{-1} and ν_s at 1376 cm^{-1} and C–H stretching vibration at 2852 cm^{-1}) [22–24]. In addition, a number of overlapping vibrations due to carbonate species are also observed in the 1100–800 cm^{-1} region and ~1500 cm^{-1} which are assigned to monodentate, bidentate, bulk carbonate and carboxylate OCO stretching vibrations [3,19,20,23,25,26].

Kim et al. proposed that carbonates and/or formates block the active sites during the water–gas shift reaction causing deactivation of Au/CeO_2 catalysts at 240 °C using a feed containing 10% CO, 22% H_2O, 43% CO_2 and 19% H_2 [2]. Therein, sintering and over-reduction were determined not to cause deactivation. The role of carbonates and/or formates in the deactivation was assessed through comparison of X-ray photoelectron spectra of the C 1s region for a fresh and deactivated catalyst which showed an increase in the peak at 288.8 eV assigned to increased carbonates. The DRIFT spectra of the fresh catalyst exposed to CO/H_2 mixture at 240 °C also showed increased intensity of bands due to formates and carbonates. Fig. 3 showed no increase in carbonate/formate bands during the reaction and no correlation between the rate of formation/amount of carbonates/formates under the WGS feed and the deactivation rate.

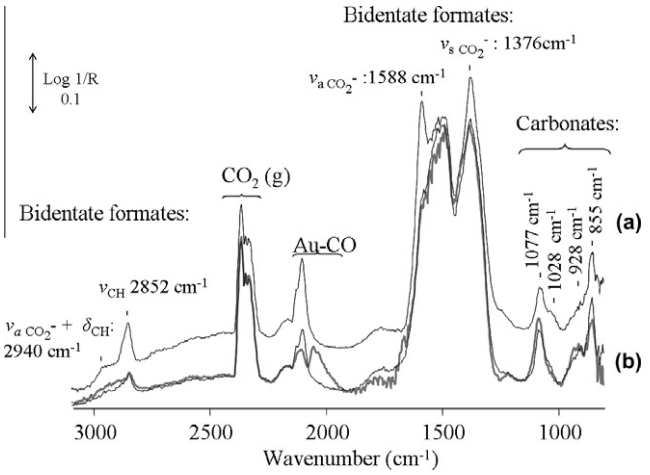

Fig. 3. DRIFT spectra recorded at 150 °C upon introduction of: (a) 1% H_2O WGS feed and (b) upon introduction of 7.5% H_2O WGS feed (dark spectrum); light spectrum after 10 h under 7.5% H_2O WGS feed.

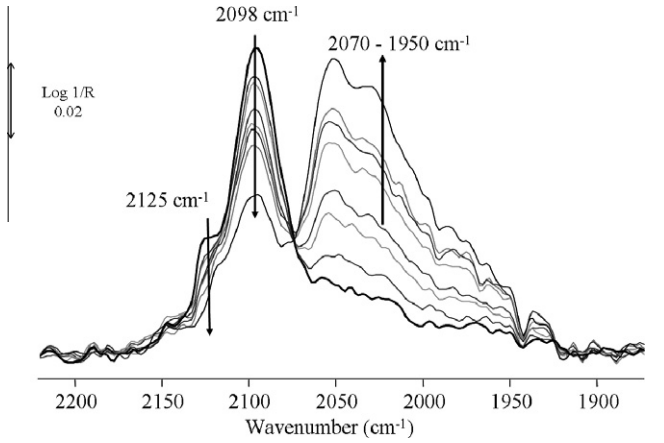

Fig. 4. DRIFT spectra of 2250–1950 cm^{-1} region focussing on the Au–CO bands; spectra shown are after 0 (bold spectrum), 1, 3, 5, 8, 10, 12 and 20 h under full WGS feed at 150 °C. All spectra have been corrected for the electronic transition of ceria reduced and unreacted gas-phase CO.

Dentwitz et al. proposed that the formation of thermally stable monodentate carbonates, under a range of conditions from idealised to realistic reaction atmospheres at 180 °C, to be the cause of deactivation of a Au/CeO_2 catalyst [3]. Infrared bands due to bidenatate and monodentate carbonates and bidentate formate species were integrated and the loss/formation recorded as a function of the feed conditions. Monodentate carbonates were observed to increase under all feeds with the increase observed to vary as the deactivation rate changed under the different conditions used. This is in contrast with the results obtained in this study where no correlation between the formation of formates/carbonates and the deactivation rate of the catalyst was obtained. The data reported, herein, are in agreement, however, with the previous study on Au/$CeZrO_4$ catalysts where no increase in activity was observed following a TPO (Temperature Programmed Oxidation) to 230 °C which suggested that deactivation is not due to adsorbed carbonaceous species [9]. This variation is possibly due to the different supports used in the studies with ceria–zirconia reported to be less sensitive to the build-up of carbonaceous species compared with ceria [27].

The region between 2200 and 1950 cm^{-1} in Fig. 3 shows strong Au–CO bands which are observed to form immediately upon exposure to the WGS feed. With CO being a reactant in the WGS reaction it is an effective probe molecule for characterising the state of the Au under reaction conditions. From Fig. 3, it is evident that after 10 h on stream there has been a significant change in the Au–CO bands in the 2200–1950 cm^{-1} region. Fig. 4 shows the spectra in the Au–CO region and Fig. 5 shows the temporal evolution of the Au–CO band areas associated with Au^0, $Au^{\delta+}$ and $Au^{\delta-}$ obtained as a function of time on stream after the introduction of the full WGS feed at 150 °C. Upon introduction of the feed, the main feature is a band at 2098 cm^{-1} which has a shoulder at higher wavenumber at 2125 cm^{-1}. The band at 2098 cm^{-1} is assigned to CO adsorbed on metallic Au particles and is consistent with spectra reported previously for Au supported on CeO_2 [23,28,29]. A band at a similar position (2110–2098 cm^{-1}) has also been observed for Au on other supports (TiO_2, ZrO_2, Al_2O_3 and Fe_2O_3) [30,31] and again was assigned to CO adsorbed on metallic Au nanoparticles, specifically at the step sites or the perimeter of Au nanoparticles [32,33]. The band at 2125 cm^{-1} is between the region where carbonyl bands due to adsorption on Au^+ (2200–2150 cm^{-1}) and Au^0 occur for oxide supported Au (2110–2090 cm^{-1}) [34]. This band is, therefore, assigned to Au which is partially oxidised, denoted as $Au^{\delta+}$. Partially oxidised Au species have been observed on Au supported on CeO_2–TiO_2 [32] and on Au/ZrO_2 [35] and have been described as being due to Au^+ atoms incorporated in a nanoparticle with the charge spread over the whole particle [34].

The identification of the major Au species from DRIFT spectroscopy as being metallic Au is consistent with previous *in situ* characterisation and DFT results for this catalyst [11]. From the previous results, a model of the active site was proposed in which a hemispherical metallic gold nanoparticle ~1 nm was anchored to the support through a gold adatom occupying a cerium lattice vacancy in the support [36]. In this case, the gold atoms in the cerium vacancy would have a partial positive charge ($Au^{\delta+}$) and the high activity of the catalyst was linked to the intimate contact of the nanoparticle with the support.

With increasing time on stream and subsequent catalyst deactivation, the DRIFT spectra showed that bands due to Au^0–CO and $Au^{\delta+}$–CO species decreased in intensity (Fig. 4). The relative intensities of these two bands were also found to change on deactivation with the $Au^{\delta+}$–CO band decreasing faster than Au^0–CO species (Fig. 5). However, if the $Au^{\delta+}$–CO species were an active site for the WGS reaction, it would be expected that the relative intensity of the bands would change in line with the deactivation rate; this was not observed. The observed $Au^{\delta+}$–CO species could be CO adsorbed on isolated Au atoms locked into the support in cerium lattice vacancies which are able to adsorb CO and but are rapidly reduced under the feed/lost in a fast initial deactivation process.

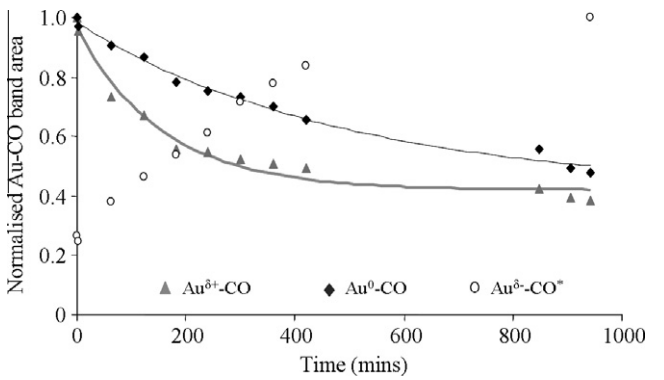

Fig. 5. Rate of change of Au–CO bands with time on stream under the full WGS feed (2% CO, 2% CO_2, 8.1% H_2 and 7.5% H_2O) at 150 °C. *Bands in 2070–1850 cm^{-1} region may be due to Au reconstruction or negatively charged Au.

In contrast, the rate of change of the Au^0–CO species did correlate with the long-term deactivation rate which suggests that metallic gold is the active species and that the perimeter sites of the nanoparticle are able to strongly adsorb CO as proposed by Goguet et al. [9]. The identification of metallic Au as the active Au species is in contrast with recent work of Deng et al. [37] who used *in situ* EXAFS and XANES to study low-loading Au/CeO_2 catalysts (<1% Au) under the WGS feed (5% CO + 3% H_2O at 100 and 200 °C). They observed reduction of Au under the WGS feed and gradual Au agglomeration with the extent of Au reduction being related to the reduction potential of the feed. The maximum activity was found for highly dispersed gold with lower activity observed when metallic Au was present.

As Au^0–CO and $Au^{\delta+}$–CO bands decreased, a new broad Au–CO band at a lower wavenumber of the metallic Au–CO band was observed to increase in intensity (Fig. 4). This broad feature, between 2070 and 1950 cm^{-1}, is located in the region where CO adsorbed on negatively charged Au has been reported on reduced Au/CeO_2 and Au/Fe_2O_3 catalysts [28–30,38,39], defect-rich Au/TiO_2 catalysts active for low-temperature CO oxidation [40] and Au on MgO surfaces [41]. The assignment of these features is still ambiguous. One possible hypothesis is that the gold nanoparticles become mobile on dewetting from the support surface during deactivation and adsorb on oxygen vacancies [42]. In these vacancies, the nanoparticles would become negatively charged through charge transfer into the nanoparticle [43]. However, a band in the 2070–1950 cm^{-1} region has also been observed on a 1 wt.% Au/Al_2O_3 catalyst following adsorption of CO at room temperature. In this case, initial CO adsorption led to a band at 2098 cm^{-1} which was assigned to CO adsorbed on kink or defect sites. Following exposure to elevated CO pressures/longer exposure times, the 2098 cm^{-1} band decreased in intensity with a new band at 2070 cm^{-1} forming which was assigned to CO adsorbed on terrace or step sites. The formation of the band at 2070 cm^{-1} was proposed to be due to a change in the adsorption site on the gold nanoparticle from the restructuring of the nanoparticle. Studies on single crystals also illustrated a shift in the CO vibrational frequency with coordination number of the Au with adsorption of CO on step, corner or terrace sites exhibiting different band positions [44,45]. Restructuring of the Au and formation of a band in the 1950–2070 cm^{-1} region has also been observed on model Au particles supported on TiO_2 where a flattening of the Au nanoparticles was observed; however, in this case the bands were assigned to adsorption on negative Au formed from electron transfer from defect-rich titania to the Au particles [46].

Clearly, in the case of the catalysts investigated in this study, the formation of the bands between 1950 and 2070 cm^{-1} showed a significant change in the adsorption sites of the Au under the WGS reaction. The formation of these bands could be due to a structural change in the nanoparticle as the catalyst deactivates with the loss of the strong CO adsorption sites at the interface of the nanoparticle and the support (Au^0–CO bands). Irrespective of the exact attribution of the origin of these bands, their increase in intensity, as the catalyst deactivates, clearly indicated that this adsorption site/state of the gold is inactive for the water–gas shift reaction.

3.3. Infrared analysis: isosteric heat of adsorption

The *in situ* DRIFT spectra shown in this study exhibit Au–CO bands which are more intense than those observed in other studies run at comparable temperatures [3]. Therefore, with the strength of the CO adsorption on the Au nanoparticle being linked to the activity of the catalyst for the water–gas shift reaction [11,47], the isosteric heat of adsorption over an active and a deactivated $Au/CeZrO_4$ catalyst was probed in order to investigate the possible correlation between the change in the strength of CO adsorption and the loss of WGS activity. A 2 wt.% Au catalyst was deactivated under the full water–gas shift feed at 150 °C for 12 h which led ca. 30% loss in activity (Fig. 1).

Clausius–Clapeyron plots of $\ln P_{(CO)}$ as a function of $1/T$ for different surface coverages of CO allowed the heat of adsorption to be obtained for an active and deactivated catalyst (data shown in the Supplementary Information). The heat of adsorption increases with decreasing CO coverage for the active catalyst and ranged from 30 to 105 kJ mol^{-1} (when extrapolated to zero coverage) and for the deactivated catalyst 10–90 kJ mol^{-1}. The heat of adsorption over the deactivated catalysts was greatly reduced and suggests that the loss of activity can be correlated with the ability of Au to adsorb CO. The lower heat of adsorption following reaction is consistent with the activity being linked with the CO chemisorption ability of the Au.

The heat of adsorption of CO at low coverage on the most active $Au/CeZrO_4$ catalyst in this study is larger than previously reported values which are typically between 45 and 70 kJ mol^{-1}, for example values for Au(3 3 2) [33] and Au(1 0 0) [48] are 55 ± 3 kJ mol^{-1} and 58 ± 3 kJ mol^{-1}, respectively. The heat of adsorption on a reconstructed Au(1 1 0)–(1 × 2) surface also has a comparable value of 59 kJ mol^{-1} [49]. DFT calculations for energy of CO adsorption on different Au surfaces showed that CO chemisorption is favoured on lower coordination sites with values of 32.8, 66.6, 75.3 and 105.2 kJ mol^{-1} for terrace sites on Au(1 1 1), step sites on Au(3 3 1), kink sites on Au(8 7 4) and Au adatoms on the Au(1 1 1) surface, respectively [44]. In the case of supported Au catalysts, Roze et al. have reported heats of adsorption of 43–62 kJ mol^{-1} for 1 wt.% Au/Al_2O_3 for a band at 2098 cm^{-1} assigned to CO adsorbed on defect/kink sites of Au [50] while Derrouiche et al. reported values of 47–74 kJ mol^{-1} for Au/TiO_2 [51].

The higher heat of adsorption of CO for our Au catalysts compared with the values reported previously for $CeZrO_4$ supported Au is consistent with the strong interaction of the Au nanoparticles with the support which significantly modifies the chemisorption properties of the metal [9]. Upon deactivation as the gold cluster becomes detached, the adsorption characteristics of the gold will be modified and changes occur both in terms of the type and in terms of the number of adsorption sites on the gold particle at positions remote from the interface. Previously, the model proposed was that interfacial gold atoms ($Au^{\delta\delta+}$) are the sites able to adsorb CO at elevated temperatures [9]. This interpretation was supported by DFT calculations, which showed that CO chemisorption is enhanced on the Au site that is near the interface between the gold and the support compared to CO chemisorption on the Au cluster without support. An important feature of this model was that the metal cluster is bound to the surface of the oxide via gold atoms ($Au^{\delta+}$) in cerium vacancies in the oxide lattice. It is the removal of these anchor points that is responsible for the dewetting of the gold cluster and the loss of the adsorptive properties and *in fine* the catalyst activity. The $Au^{\delta\delta+}$ sites proposed in the previous study were assigned as the perimeter sites of the nanoparticle, which more correctly corresponds with the Au^0–CO bands observed by DRIFTS.

3.4. Effect of water concentration in feed

The DRIFT spectra under the 1% water feed exhibited the same Au–CO bands as that observed under the feed containing the higher water concentration with bands due to Au^0–CO at 2098 cm^{-1} and $Au^{\delta+}$–CO at 2125 cm^{-1}. Under the lower water concentration feed, the Au–CO bands are more intense. This is consistent with the reaction being positive order with respect to the water and non-zero order with respect to CO under the investigated reaction conditions explored. Such conditions lead to a higher equilibrium

concentration of CO adsorbed on the Au with decreasing water concentration as observed.

During the reaction using the 1% water feed, the Au^0–CO and $Au^{\delta+}$–CO species are again observed to decrease with time on stream and the broad band between 2070 and 1950 cm^{-1} observed to increase. Fig. 6 shows the temporal evolution of the Au–CO bands area with time on stream for WGS reaction conditions using 1% and 7.5% water. Clearly, the rate of decrease was lower for the conditions using 1% compared with 7.5% water corresponding with the lower deactivation rate observed for reaction under the 1% water feed of 0.01% h^{-1} (compared to 0.23% h^{-1} for the full WGS feed). Under both water feeds, the $Au^{\delta+}$–CO species decreased more rapidly than found for the Au^0–CO species. Again, the $Au^{\delta+}$–CO species are lost faster than the rate of deactivation while the Au^0–CO species correlates well with the loss of CO conversion.

3.5. Removal of H_2 and CO_2 from the feed – activity data

It was already reported that the deactivation rate is linearly related to the water concentration of the feed [9] but little investigation has been reported as to how the other components of the WGS feed affected the stability [24]. Following the reaction under the full WGS feed in the microreactor system, CO_2 and then H_2 were removed from the feed to investigate whether the presence of these components influenced the stability.

Fig. 7 shows the sequential exposure of the catalyst to the full WGS feed, CO_2-free feed and H_2-free feed at 140 °C. After 20 h of reaction under the full WGS feed, the CO_2 was removed from the feed and the helium balance increased to maintain the feed concentrations. The conversion was found to increase highlighting an inhibition effect of CO_2; however, in addition, under the CO_2-free feed it was observed that the catalyst showed little on-stream deactivation. To determine whether the stability enhancement was permanent, CO_2 was re-introduced and the reaction monitored for a further 10 h. The presence of CO_2 in the feed clearly reduced the stability of the catalyst with the deactivation rate returning to that obtained initially under the full feed. The catalyst, upon re-introduction of CO_2 to the feed (after ~45 h total reaction time under a WGS feed), also exhibits higher activity than would be obtained following 45 h of reaction under the full WGS feed. 30% CO conversion was found following the CO_2-free feed pre-treatment compared with ~20% CO conversion under the same total reaction time under the full WGS feed (Fig. 7). The effect of H_2 was then investigated in an analogous method to that of CO_2. Removal of H_2 from the feed led to an increase in the CO conversion evidencing an inhibition effect of H_2 but no enhancement in the stability of the catalyst relative to that found under the full WGS feed was observed. The same series of feed conditions was repeated at 200 °C and again, significant enhancement of the catalyst stability was observed upon removal of CO_2.

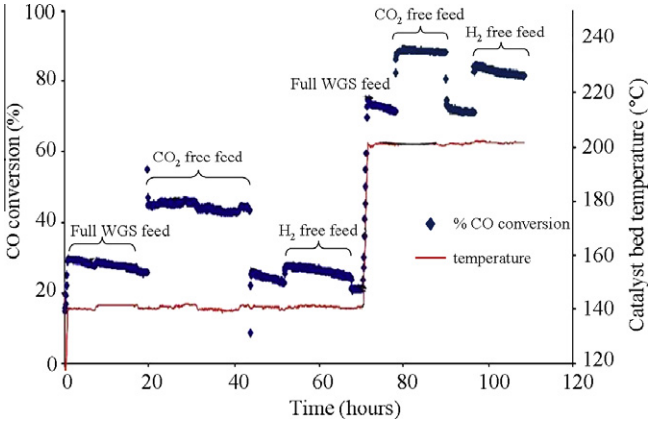

Fig. 7. Effect on CO conversion of removing H_2 and CO_2 from the WGS feed at 140 and 200 °C.

With the enhanced stability observed following CO_2 removal from the feed (deactivation rate of 0.07% h^{-1}), further testing was carried out with a WGS feed without additional CO_2 added (feed containing $CO + H_2O + H_2$). Fig. 8 compares the activity of a 1 wt.% $Au/CeZrO_4$ under the CO_2-free feed and the full WGS feed at 150 °C. Under the CO_2-free feed there was only a slight enhancement in stability which could be due to the varied feed composition changing the position of the equilibrium resulting in higher conversion of water to hydrogen and hence a lower surface water concentration and slower hydrolysis of the Au–support interface which has been postulated as leading to the catalyst deactivation [9]. This small change in stability is in contrast with the significant enhancement in stability obtained when CO_2 was removed from the feed *after* the catalyst had had prior exposure to the full WGS feed. In order to probe this in more detail, an investigation into pre-treatment of the catalyst was explored.

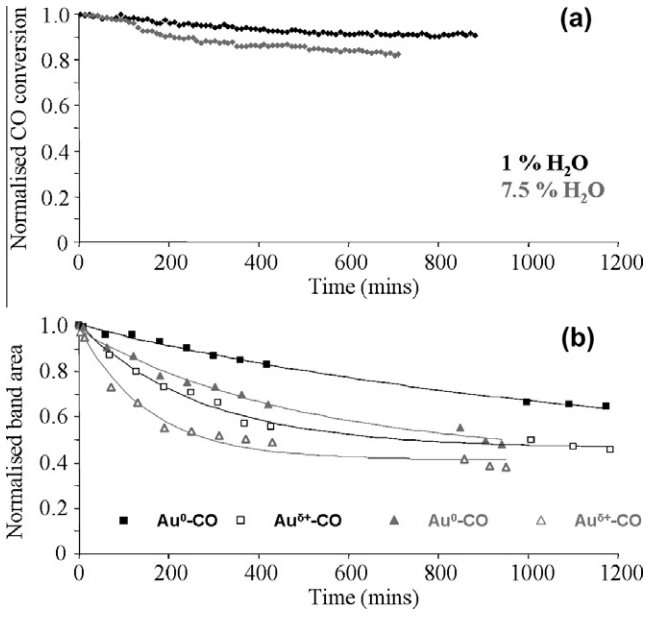

Fig. 6. Comparison of rate of change of Au–CO bands with time on stream under the full WGS feed (2% CO, 2% CO_2, 8.1% H_2 and 7.5% H_2O) and low water feed (2% CO, 2% CO_2, 8.1% H_2 and 1.0% H_2O) for a 1 wt.% $Au/CeZrO_4$ catalyst.

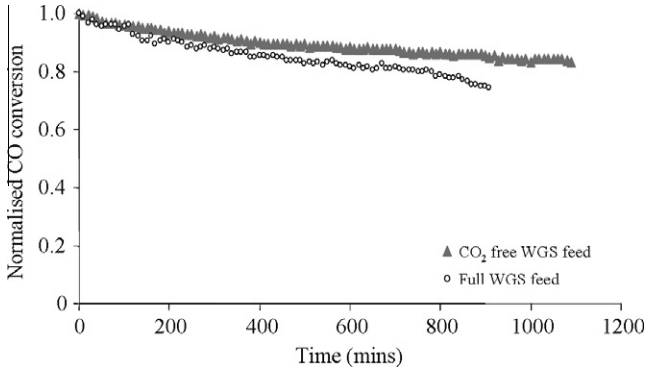

Fig. 8. Normalised CO conversion for WGS reaction at 150 °C under CO_2-free feed (2% CO, 8.1% H_2 and 7.5% H_2O, balance He) and the full WGS feed (2% CO, 2% CO_2, 8.1% H_2 and 7.5% H_2O).

A reaction was carried out where a 1 wt.% $Au/CeZrO_4$ catalyst was exposed to the full WGS feed at 200 °C for 1 h as a pre-treatment. Following the pre-treatment, the temperature was lowered to 100 °C under He before introduction of a CO_2-free WGS feed and the temperature increased to 150 °C. The reaction was monitored with DRIFTS-GC during the pre-treatment and the reaction. Fig. 9 shows a comparison of the activity and the Au^0–CO integrated band area under a CO_2-free feed with and without pre-treatment under the full WGS feed. It is evident that pre-treatment of the catalyst and then reaction under a CO_2-free feed does led to an enhancement in the stability which is also reflected in the slower rate of loss of Au^0–CO bands.

The DRIFTS results showed that the rate of change of Au^0–CO species followed the trend in stability with feed conditions (Fig. 9). No $Au^{\delta+}$–CO bands were observed under the CO_2-free feed following the pre-treatment at 200 °C under the full WGS feed. During the full WGS pre-treatment temperature ramp to 200 °C, the band due to $Au^{\delta+}$–CO species was depleted and was no longer evident at 200 °C under the feed. In fact, at 200 °C, under all feeds, only Au^0–CO bands were observed. As demonstrated already, the $Au^{\delta+}$–CO species are significantly less stable than Au^0–CO species and while $Au^{\delta+}$ species may have high activity for the WGS reaction they are not observed after pre-treatment of the catalyst when the catalyst is still very active and stable. Only Au^0–CO bands were observed under the CO_2-free feed (after pre-treatment) and their rate of change corresponded with the deactivation rate as observed under other feed conditions tested.

Alternative pre-treatments were also explored to determine whether further enhancement could be obtained. Fig. 10 shows the activity data obtained for reaction at 150 °C under a CO_2-free feed following pre-treatment with water, hydrogen, CO_2, water plus CO_2 and carbonic acid. Carbonic acid was examined to test the postulation that the effect of CO_2 in the feed could be related to its interaction with water to form carbonic acid. Pre-treatment at 200 °C with hydrogen, water or CO_2 did not have any effect on the stability with a deactivation rate comparable to that observed in reaction under the full WGS feed. Pre-treatment with a simultaneous feed of water and CO_2 caused faster deactivation than water or carbon dioxide alone. The stability also varied with the proportion of CO_2 in the water mixture with faster deactivation being observed when the catalyst was pre-treated with 10% CO_2 plus 7.5% water compared with a feed containing 5% CO_2 plus 7.5% water. The deactivation rate was faster again following carbonic acid treatment.

Although the variation in the CO_2 concentration of the feed has been previously reported to correlate with deactivation [3], in this study, removal of CO_2 from the feed enhances stability. Under these varied feed conditions there was again no correlation

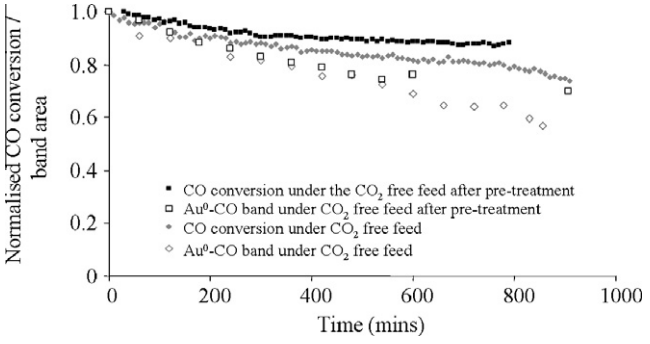

Fig. 9. Normalised CO conversion and Au^0–CO band area during reactions at 150 °C under a CO_2-free WGS feed (2% CO, 8.1% H_2 and 7.5% H_2O) with and without pre-treatment with the full WGS feed (2% CO, 2% CO_2, 8.1% H_2 and 7.5% H_2O).

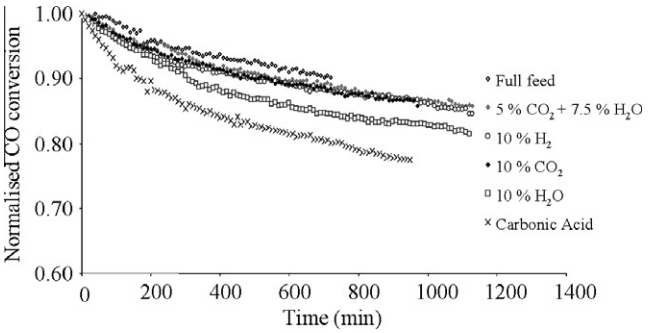

Fig. 10. Reaction of a 1 wt.% $Au/CeZrO_4$ catalyst under a CO_2-free WGS feed (2% CO, 8.1% H_2 and 7.5% H_2O) at 200 °C following different pre-treatments at 200 °C. The effect of pre-treating the catalyst with the full WGS feed (2% CO, 2% CO_2, 8.1% H_2 and 7.5% H_2O), 10% CO_2, 10% H_2, 10% H_2O, 5% CO_2 + 7.5% H_2O and carbonic acid.

between carbonates/formates surface concentration and the observed deactivation rate. In addition, surprisingly, running the reaction initially without CO_2 in the feed did not lead to the same enhanced stability. Therefore, it is possible that CO_2 is required initially to form the active catalyst but that prolonged exposure to elevated amounts of CO_2 in the presence of water influences the structure of the Au nanoparticle and enhances the dewetting of the nanoparticle from the support.

3.6. Effect of reaction temperature

Previously it was reported that elevated reaction temperatures (>250 °C) led to rapid and irreversible deactivation [9]. In order to investigate the impact of thermal deactivation on the various Au–CO species, the reaction temperature was cycled between 150 °C and 400 °C while recording DRIFT spectra during the reaction cycles at 150 °C. Fig. 11 shows the normalised CO conversion, $Au^{\delta+}$–CO and Au^0–CO band areas as a function of time following cycles between 150 and 400 °C. Following the first temperature cycle to 400 °C, a significant loss in activity of ~50% was observed. After this initial rapid loss of activity, the $Au^{\delta+}$–CO band was no longer observed which was consistent with loss of $Au^{\delta+}$–CO following the pre-treatment at 200 °C, as discussed above. With the loss of activity, there was also a corresponding decrease in the Au^0–CO band at 2098 cm^{-1}. With subsequent cycles at 400 °C, further decreases in conversion were observed with concomitant decreases in the intensity of the Au^0–CO band. These results showed once again that the loss of the metallic Au adsorption sites can be correlated with the long-term deactivation of the catalyst which suggests a common deactivation mechanism. Further evidence for the rate of reaction correlating with the Au^0–CO band area is shown in the inset of Fig. 11 where a plot of rate of reaction/Au^0–CO band area gives a constant value (within experimental error). This shows that as the reaction progresses and the catalyst deactivates, the loss of band area of Au^0–CO species correlates with the deactivation rate and further suggests a change in the CO chemisorption ability of the Au to be related to the catalyst deactivation.

It is interesting to note that following the rapid thermal deactivation, no bands in the 2070–1950 cm^{-1} region were formed. If these species were due to adsorption of CO on negatively charged Au formed from the nanoparticle adsorption on an oxygen vacancy, increased temperature would be expected to increase the number of oxygen vacancies. Consequently, more negatively charged Au would be expected to form as the catalyst deactivates; this is obviously not the case. As reported previously [9], deactivation at low temperatures is likely due to hydrolysis of the gold nanoparticle/support interaction causing a change in shape/structure of the

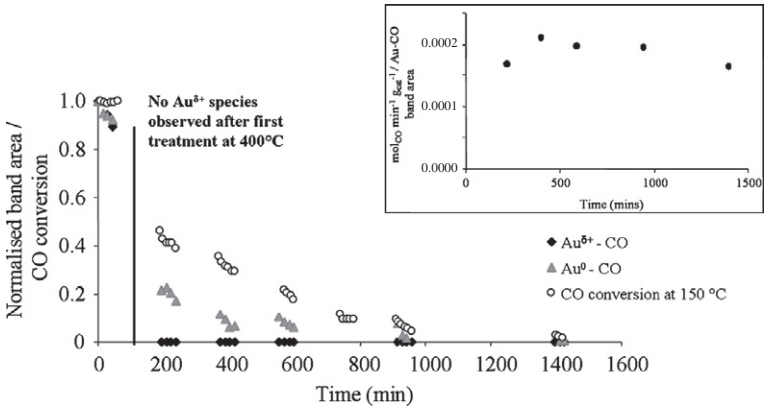

Fig. 11. Comparison of catalyst activity and rate of change of Au–CO species at 150 °C following hour intervals under the full WGS feed (2% CO, 2% CO_2, 8.1% H_2 and 7.5% H_2O) at 400 °C. The inset shows a plot of the rate of reaction ($mol_{CO}\ min^{-1}\ g_{cat}^{-1}$)/$Au^0$–CO band area with reaction time.

nanoparticle with the gold nanoparticle reconstructing and progressively losing the intimate contact with the support [9]. This is supported by the formation of the Au–CO bands in the 2070–1950 cm^{-1} region and these bands being attributed to particle reconstruction similar to that described in Roze et al. [50]. However, with the thermal deactivation, a more extreme change in the structure of the nanoparticle could be responsible for the greater and more rapid loss of activity and the corresponding different CO adsorption behaviour compared to reaction at lower temperatures.

4. Conclusions

The adsorption of CO as a probe of the state of the Au is a widely used technique which was well suited for this study because of the strong CO chemisorption ability of these Au catalysts. The high heats of adsorption (90–105 kJ mol^{-1}) is consistent with the intense Au–CO bands observed at the reaction temperature of 150 °C and which allowed investigation into the Au species under relevant conditions and monitoring of the change of these species with time on stream. This DRIFTS-GC study under varying feed conditions/reaction temperatures has shown metallic Au to be the important species for the WGS reaction. $Au^{\delta+}$ species were shown to be less stable under the feed and were no longer observed at reaction temperatures above 200 °C when the catalyst was still active. It is unlikely that a very low number (below detection limit of DRIFTS technique) of extremely active sites could be responsible for the high WGS activity observed. This is because the rate of change of positively charged species did not match the long-term deactivation rate while the change of Au^0–CO species did correlate well under all feed/reaction conditions explored.

It is proposed that formation of the $Au^{\delta-}$ species are in fact due to a change in the adsorption site due to the restructuring of the Au under the WGS feed during the progressive dewetting of the gold nanoparticle which is the deactivation mechanism proposed for these catalysts. In this work, negatively charged Au species were not observed following the high-temperature WGS reaction when more oxygen vacancies would be expected. This result suggests that the bands in the 2070–1950 cm^{-1} region may be related to a restructuring of the Au rather than CO adsorption on negatively charge gold species.

A reversible effect on the stability was observed upon removal and re-introduction of CO_2 into the feed. The thermal deactivation was irreversible [9,11] and significantly faster than the deactivation observed on 1 wt.% Au/$CeZrO_4$ under varied feed conditions. Hence, while there may be a common deactivation mechanism, the rate at which the structural change occurs may be correlated with the changing CO sorption ability of the Au under the different reaction conditions as observed by DRIFTS.

The activity and stability of these Au/$CeZrO_4$ catalysts are very sensitive to the feed composition. An initial period of reaction under the full WGS feed is required before removing the CO_2 from the feed in order to obtain enhanced stability of these catalysts. Therefore, it is proposed that the active Au sites are formed under the full WGS feed wherein the Au nanoparticles are locked into the support. Once the nanoparticles have formed, the feed composition and reaction temperature will determine the rate at which the nanoparticles become detached from the surface, with contact with water leading to hydrolysis of the nanoparticle/support interaction. During reaction under the CO_2-free feed, the surface concentration of water will be reduced (equilibrium shifting towards hydrogen formation) which is one factor which could account for the slower deactivation when CO_2 is removed from the feed. However, faster deactivation is observed when the catalyst is pre-treated with $CO_2 + H_2O$ or carbonic acid rather than with water alone. This enhanced deactivation from the combined effect of CO_2 and water may be the formation of species such as H_3O^+/HCO_3^- which may promote the dewetting of the nanoparticle through acid/base-mediated hydrolysis. Therefore, removal of the CO_2 once the active state of the catalyst has been achieved greatly improves the stability.

The use of these catalysts with membrane reactors where CO_2 could be removed from the feed to provide a highly active and stable catalyst provides great potential for the long-term use of Au catalysts in the production of hydrogen.

Acknowledgment

We would like to thank the EPSRC for funding as part of the CARMAC and CASTech projects.

Appendix A. Supplementary material

Supplementary data associated with this article can be found, in the online version, at doi:10.1016/j.jcat.2010.05.021.

References

[1] A.A. Fonseca, J.M. Fisher, D. Ozkaya, M.D. Shannon, D. Thompsett, Top. Catal. 44 (2007) 223.
[2] C.H. Kim, L.T. Thompson, J. Catal. 230 (2005) 66.
[3] Y. Denkwitz, A. Karpenko, V. Plzak, R. Leppelt, B. Schumacher, R.J. Behm, J. Catal. 246 (2007) 74.
[4] M.M. Schubert, V. Plzak, J. Garche, R.J. Behm, Catal. Lett. 76 (2001) 143.

[5] M.M. Schubert, A. Venugopal, M.J. Kahlich, V. Plzak, R.J. Behm, J. Catal. 222 (2004) 32.
[6] W. Deng, J. De Jesus, H. Saltsburg, M. Flytzani-Stephanopoulos, Appl. Catal. A 291 (2005) 126.
[7] A. Luengnaruemitchai, S. Osuwan, E. Gulari, Catal. Commun. 4 (2003) 215.
[8] Q. Fu, W. Deng, H. Saltsburg, M. Flytzani-Stephanopoulos, Appl. Catal. B 56 (2005) 57.
[9] A. Goguet, R. Burch, Y. Chen, C. Hardacre, P. Hu, R.W. Joyner, F.C. Meunier, B.S. Mun, D. Thompsett, D. Tibiletti, J. Phys. Chem. C 111 (2007) 16927.
[10] Q. Fu, H. Saltsburg, M. Flytzani-Stephanopoulos, Science 301 (2003) 935.
[11] D. Tibiletti, A.A. Fonseca, R. Burch, Y. Chen, J.M. Fisher, A. Goguet, C. Hardacre, P. Hu, D. Thompsett, J. Phys. Chem. B 109 (2005) 22553.
[12] C.H. Kim, L.T. Thompson, J. Catal. 244 (2006) 248.
[13] J. Rodriguez, X. Wang, P. Liu, W. Wen, J. Hanson, J. Hrbek, M. Pérez, J. Evans, Top. Catal. 44 (2007) 73.
[14] F.C. Meunier, D. Reid, A. Goguet, S. Shekhtman, C. Hardacre, R. Burch, W. Deng, M. Flytzani-Stephanopoulos, J. Catal. 247 (2007) 277.
[15] F.C. Meunier, A. Goguet, S. Shekhtman, D. Rooney, H. Daly, Appl. Catal. A 340 (2008) 196.
[16] J. Sirita, S. Phanichphant, F.C. Meunier, Anal. Chem. 79 (2007) 3912.
[17] J. Couble, P. Gravejat, F. Gaillard, D. Bianchi, Appl. Catal. A 371 (2009) 99.
[18] C. Binet, A. Badri, J.C. Lavalley, J. Phys. Chem. 98 (1994) 6392.
[19] C. Binet, M. Daturi, J.C. Lavalley, Catal. Today 50 (1999) 207.
[20] F. Bozon-Verduraz, A. Bensalem, J. Chem. Soc. Faraday Trans. 90 (1994) 653.
[21] H. Daly, J. Ni, D. Thompsett, F.C. Meunier, J. Catal. 254 (2008) 238.
[22] G. Busca, J. Lamotte, J.C. Lavalley, V. Lorenzelli, J. Am. Chem. Soc. 109 (1987) 5197.
[23] A. Abd El-Moemen, A. Karpenko, Y. Denkwitz, R.J. Behm, J. Power Sources 190 (2009) 64.
[24] A. Abd El-Moemen, G. Kucerová, R.J. Behm, Appl. Catal. B 95 (2010) 57.
[25] C. Li, Y. Sakata, T. Arai, K. Domen, K. Maruya, T. Onishi, J. Chem. Soc. Faraday Trans. 85 (1989) 929.
[26] B. Aeijelts Averink Silberova, G. Mul, M. Makkee, J.A. Moulijn, J. Catal. 243 (2006) 171.
[27] C.H. Kim, L.T. Thompson at GOLD2006: New Industrial Applications for Gold, Limerick, Ireland, 2006.
[28] T. Tabakova, F. Boccuzzi, M. Manzoli, D. Andreeva, Appl. Catal. A 252 (2003) 385.
[29] M. Manzoli, F. Boccuzzi, A. Chiorino, F. Vindigni, W. Deng, M. Flytzani-Stephanopoulos, J. Catal. 245 (2007) 308.
[30] F. Menegazzo, M. Manzoli, A. Chiorino, F. Boccuzzi, T. Tabakova, M. Signoretto, F. Pinna, N. Pernicone, J. Catal. 237 (2006) 431.
[31] Y.Z. Chen, B.J. Liaw, W.C. Chang, C.T. Huang, Int. J. Hydrogen Energy 32 (2007) 4550.
[32] A. Chiorino, M. Manzoli, F. Menegazzo, M. Signoretto, F. Vindigni, F. Pinna, F. Boccuzzi, J. Catal. 262 (2009) 169.
[33] C. Ruggiero, P. Hollins, Surf. Sci. 377–379 (1997) 583.
[34] M. Mihaylov, H. Knözinger, K. Hadjiivanov, B.C. Gates, Chem. Ing. Tech. 79 (2007) 795.
[35] F. Boccuzzi, G. Cerrato, F. Pinna, G. Strukul, J. Phys. Chem. B 102 (1998) 5733.
[36] Y. Chen, P. Hu, M.H. Lee, H. Wang, Surf. Sci. 602 (2008) 1736.
[37] W. Deng, A.I. Frenkel, R. Si, M. Flytzani-Stephanopoulos, J. Phys. Chem. C 112 (2008) 12834.
[38] F. Boccuzzi, A. Chiorino, M. Manzoli, D. Andreeva, T. Tabakova, J. Catal. 188 (1999) 176.
[39] M. Date, H. Imai, S. Tsubota, M. Haruta, Catal. Today 122 (2007) 222.
[40] T. Diemant, Z. Zhao, H. Rauscher, J. Bansmanna, R.J. Behm, Top. Catal. 44 (2007) 83.
[41] B. Yoon, H. Hakkinen, U. Landman, A.S. Worz, J.M. Antonietti, S. Abbet, K. Judai, U. Heiz, Science 307 (2005) 403.
[42] H.L. Chen, W.T. Peng, J.J. Ho, H.M. Hsieh, Chem. Phys. 348 (2008) 161.
[43] M. Sterrer, T. Risse, H.J. Freund, Appl. Catal. A 307 (2006) 58.
[44] L. Piccolo, D. Loffreda, F.J. Cadete Santos Aires, C. Deranlot, Y. Jugnet, P. Sautet, J.C. Bertolini, Surf. Sci. 566–568 (2004) 995.
[45] P. Hollins, Surf. Sci. Rep. 16 (1992) 53.
[46] T. Diemant, H. Hartmann, J. Bansmann, R.J. Behm, J. Catal. 252 (2007) 171.
[47] D.C. Grenoble, M.M. Estadt, D.F. Ollis, J. Catal. 67 (1981) 90.
[48] G. Mcelhiney, J. Pritchard, Surf. Sci. 60 (1976) 397.
[49] J.M. Gottfried, K.J. Schmidt, S.L.M. Schroeder, K. Christmann, Surf. Sci. 536 (2003) 206.
[50] E. Roze, P. Gravejat, E. Quinet, J.L. Rousset, D. Bianchi, J. Phys. Chem. C 113 (2009) 1037.
[51] S. Derrouiche, P. Gravejat, D. Bianchi, J. Am. Chem. Soc. 126 (2004) 13010.